JOM, Vol. 72, No. 11, 2020
https://doi.org/10.1007/s11837-020-04365-4

Rate Theory Model of Irradiation-Induced Solute Clustering in b.c.c. Fe-Based Alloys

MATTHEW J. SWENSON [1,3] and JANELLE P. WHARRY[2]

1.—University of Idaho, 875 Perimeter Drive, Moscow, ID 83844, USA. 2.—Purdue University, 400 Central Drive, West Lafayette, IN 47907, USA. 3.—e-mail: swenson@uidaho.edu

Solute nanoclusters are critical to the structural and mechanical integrity of numerous alloys based on the b.c.c. Fe matrix, which have risen to prominence as candidates for advanced nuclear reactor applications. Because irradiation can profoundly alter the morphology and composition of these solute nanoclusters, it is critical to understand and predict solute clustering behavior in the presence of irradiation. In this study, we advance a simple theory to model irradiation-induced nanocluster evolution subject to different irradiating particles. The model is trained and validated with experimental data following an approach similar to training a machine learning algorithm, resulting in an agile model that can be used for rapid screening of new alloys. Using the model, nanocluster evolution is found to depend upon the disordering parameter (i.e., cluster morphology and dose rate) and irradiation temperature, and is most sensitive to the solute migration, vacancy formation, and vacancy migration energies. Results are discussed with respect to the irradiation temperature shift for varying irradiating particle types and dose rates.

INTRODUCTION

Numerous alloys based on the b.c.c. Fe matrix have risen to prominence as candidates for advanced nuclear reactor applications. These alloys are known for their high-temperature strength and dimensional stability under irradiation, often attributed to their high sink strengths. In particular, nanofeatured ferritic alloys (NFAs), including oxide dispersion strengthened (ODS) alloys, contain a high density of nanoscale secondary phases, such as Ti-Y-O-rich oxides, which: (a) act as localized sinks for point defects, providing resistance to irradiation swelling,[1–8] and (b) strengthen the material without significantly compromising ductility. However, to date, studies evaluating the stability of Y-Ti-O-rich nanoclusters in ODS alloys have shown that irradiation has a considerable influence on their stability, coarsening, or dissolution behavior.[9] Other b.c.c. Fe-based alloy systems, including ferritic-martensitic (F/M) and reactor pressure vessel (RPV) steels do not contain any pre-existing nanoclusters, but can experience nucleation and growth of nanoclusters rich in Si-Mn-Ni solutes[10–14] or Cu-rich precipitates[15,16] under certain irradiation conditions. While these irradiation-induced solute clusters may yield benefits for irradiation resistance, they have also been shown to cause detrimental embrittlement, jeopardizing their long-term effectiveness in an irradiation environment.[17,18]

For these alloys, it is critical to gain a clear understanding of the solute clustering behavior in the presence of irradiation to ensure they will succeed in advanced reactor applications. A large collection of experiments in the archival literature have been conducted to evaluate solute cluster evolution (or stability) in ODS alloys, and nucleation and growth in F/M and RPV steels. In some cases, charged particle irradiations are used as surrogates for neutron irradiation. However, the irradiation dose rate, damage cascade morphologies and depth profiles all differ widely between protons, self-ions, and neutrons. Currently, there is limited understanding of the significance of these physical differences and how they influence resultant microstructure and mechanical properties of target alloys. Experiments to date have demonstrated varying results depending on the irradiating particle type.[19,20] To gain a comprehensive

(Received June 4, 2020; accepted August 26, 2020; published online September 17, 2020)

understanding of irradiation-induced solute clustering behavior, advanced multi-physics models are needed to capture the mechanisms governing these behaviors.

Several models have been presented and continue to be under development to elucidate the irradiation-induced nanocluster evolution mechanisms, including recent models using atomically based continuum, low-temperature expansion, or cluster dynamics.[21–23] Each of these models capture the physics of clustering under irradiation. However, these models are generally computationally intensive, requiring days to months to execute each iteration and evaluate the sensitivity of variables.[21,22] Plus, for many of these models, the calculation becomes overly cumbersome when applied to alloys containing multiple species of clustering solutes such as ODS (Y, Ti, and O) or F/M (Si, Mn, Ni, and Cu) alloys.[21,22] Therefore, a simplified rate theory approach, which can be applied and adapted quickly for various conditions could provide valuable insight and enable reasonably quick screening to accelerate alloy development. Similar simplifications to rate theory have successfully been employed to predict other nuclear materials phenomena, such as radiation-induced segregation (RIS) in austenitic[24] and F/M[25,26] steels.

A seminal theory for describing the mechanisms of irradiation-induced nanocluster evolution was developed by Nelson, Hudson, and Mazey (NHM)[27] using rate theory equations combined with either recoil or disordering dissolution effects from irradiation. Historically, application of this theory has likely been limited due to difficulty in accurately measuring the complex matrix and nanocluster chemical information required for input. However, more recent advancement of atom probe tomography (APT) and chemical analysis capabilities render the model potentially more useful.

The objective of this manuscript was to advance a model based on the NHM theory, to provide reasonable predictions and sensitivity analysis for experimentally observed nanocluster irradiation evolution. Experimental data from Refs. 13 and 19 for a model ODS alloy and the commercial F/M alloy HCM12A were used to train and validate the model—this approach is consistent with those used for training machine learning algorithms, albeit with a limited data set. In each alloy, we observed how cluster evolution varies with different irradiating particles, showing apparent dependencies on dose rate and damage cascade morphology. Such varying cluster evolution behavior provides ample opportunity to evaluate the sensitivity of several variables.

COMPUTATIONAL METHOD

The modeling is based on the theory developed by Nelson et al.,[27] considering multiple radiation effects occurring simultaneously and their combined influence on the relative size of nanoclusters within the alloy matrix. For model integrity, it is desirable to have as much experimental data as possible. Irradiation experiments on the same heats of a model Fe-9%Cr ODS alloy and the commercial F/M alloy HCM12A are presented in Refs.13 and 19, with alloy compositions provided in Table I. In these studies, atom probe tomography is used to characterize the average size, number density, and volume fraction of Y-Ti-O-rich, or Si-Mn-Ni-rich and Cu-rich nanoclusters following each irradiation. The data from these studies is summarized in Table II, providing a more complete picture of nanocluster evolution and enabling a comprehensive analysis using the model.

The NHM Theory

The advanced Nelson-Hudson-Mazey (NHM) theory is introduced in Ref. 27 as a set of first-order differential equations describing the change in precipitate radius over a unit of time. Here, the same equations are applied to describe nanoclusters in the alloys, which may not be true stoichiometric secondary phases. The NHM equation is derived to account for two separate mechanisms of dissolution of nanocluster phases: (a) recoil dissolution, and (b) disordering dissolution. A recent review of nanocluster evolution in ODS alloys[9] suggests these mechanisms act concurrently during irradiation, so the NHM theory appropriately considers both mechanisms within a combined equation:

$$\frac{dr}{dt} = -\frac{\phi}{N} - \psi K + \frac{3D^{irr}C}{4\pi pr} - D^{irr}r^2 n \qquad (1)$$

The first two terms on the right-hand side represent the effects of recoil and disordering dissolution,

Table I. Chemical composition of Fe-9%Cr ODS and HCM12A (wt.%)

Element	Fe-9%Cr ODS	HCM12A
Cr	8.60	10.83
Mo	–	0.3
Mn	0.05	0.64
Ni	0.06	0.39
V	–	0.19
Cu	–	1.02
W	1.95	1.89
Si	0.048	0.27
Nb	–	0.054
C	0.14	0.11
N	0.017	0.063
Al	–	0.001
P	< 0.005	0.016
S	0.003	0.002
Ti	0.23	–
Y	0.27	–
O	0.14	–
Ar	0.004	–
Fe	Bal.	Bal.

Table II. Summary of nanocluster morphology in Fe-9%Cr ODS and HCM12A used for this study

Nanoclusters	As received	Fe^{2+} ion-irradiated (500°C)			Proton-irradiated (400°C)			Proton-irradiated (500°C)			Neutron-irradiated (500°C) 3 dpa
Source	Ref. 19	1 dpa Ref. 19	3 dpa Ref. 19	100 dpa Ref. 19	3 dpa Ref. 13	7 dpa Ref. 13	10 dpa Ref. 13	1 dpa Ref. 19	2.4 dpa Ref. 19	7 dpa Refs. 13,19	Ref. 19
Fe-9%Cr ODS (Y-Ti-O clusters)											
Average diameter, D_G (nm)	5.71	6.20	5.73	5.58	–	–	–	5.52	5.15	5.40 Ref. 19	5.03
SD of the mean (nm)	± 0.09	± 0.09	± 0.11	± 0.06	–	–	–	± 0.13	± 0.04	± 0.07 Ref. 19	± 0.08
Number density, N_{nc} ($\times 10^{21}$ m^{-3})	443	131	120	433	–	–	–	156	414	226 Ref. 19	152
Volume fraction, f_v (%)	4.1	3.7	3.6	3.8	–	–	–	3.3	4.1	4.4 Ref. 19	2.0
HCM12A (Si-Mn-Ni clusters)											
Average diameter, D_G (nm)	–	–	5.95	–	4.2	4.6	5.0	–	9.63	7.2 Ref. 13	4.36
SD of the mean (nm)	–	–	± 0.23	–	± 0.2	± 0.2	± 0.4	–	± 0.43	± 0.4 Ref. 13	± 0.05
Number density, N_{nc} ($\times 10^{21}$ m^{-3})	–	–	92	–	232	269	271	–	19	43 Ref. 13	398
Volume fraction, f_v (%)	–	–	1.1	–	0.9	1.37	1.77	–	1.9	0.84 Ref. 13	2.8
HCM12A (Cu-rich clusters)											
Average diameter, D_G (nm)	–	–	6.18	–	3.4	4.0	1.9	5.03	6.82	6.6 Ref. 13	4.59
SD of the mean (nm)	–	–	± 0.13	–	0.4	0.2	0.4	± 0.07	± 0.32	± 0.4 Ref. 13	± 0.06
Number density, N_{nc} ($\times 10^{21}$ m^{-3})	–	–	107	–	427	296	239	179	19	37 Ref. 13	372
Volume fraction, f_v (%)	–	–	2.5	–	0.88	0.99	0.69	2.6	1.5	0.56 Ref. 13	3.1

respectively. Each of these terms is preceded with a negative sign, representing a reduction in cluster radius from irradiation. These terms include the flux of recoil atoms across the nanocluster interface (ϕ), dose rate (K), atomic density of the target alloy (N), and the disordering parameter (ψ) for the irradiation. The disordering parameter is the product of the effective diameter of the damage cascade (l) and the relative efficiency (f) at which irradiation generates re-dissolved solutes.[27] The third and fourth terms in Eq. 1 represent the balance of solute migration from the matrix to the nanocluster, resulting in net growth of the cluster size. They include the radiation-enhanced diffusion (RED) rate of the solutes (D^{irr}), the total non-carbide composition of each of the clustering species (C), the percentage of clustered atoms which are the solute species (p), the average radius of the nanoclusters (r), and the number density of clusters (n). In its entirety, the calculation may result in either a positive or negative change in radius over time, depending on the input values of each variable.

Most of these parameters may be measured or reasonably estimated for a specific alloy system under investigation. The one exception is the disordering efficiency parameter (f). In fact, Nelson et al. acknowledge that the disordering efficiency is the least understood variable in their model and suggest this parameter could be fitted to experimental data to determine an estimated value for different irradiation conditions.[27] This is the approach taken in our application of Eq. 1. In the following sections, we outline the modeling approach to simulate nanocluster size evolution and the potential usefulness of the model through sensitivity analysis.

Modeling Approach, Inputs, and Calculation Loop

The first term on the right hand side of Eq. 1 represents recoil dissolution, and ϕ may be estimated as $\phi = K \cdot 10^{14}$.[27] For this study, the dose rates (K) for the Fe^{2+}, proton, and neutron irradiation are 2.2×10^{-4} dpa/s, $\sim 10^{-5}$ dpa/s, and $\sim 10^{-7}$ dpa/s, respectively,[19] while N represents the atomic density of the target alloy (85.2 atoms/nm^3).

The last two terms on the right-hand side of Eq. 1 contain the variables r, n, p, and C. The value for the average cluster radius, r, is calculated as $r = 1/2\, D_G$, where D_G is the average cluster Guinier diameter of the as-received alloy (Table I). Meanwhile, n represents the number density and values for p and C are acquired through APT analysis. From the composition data of the clusters, p is calculated as:

$$p_{\text{cl}}^{j} = \frac{N_{\text{cl}}^{j}}{\sum N_{\text{cl}}} \tag{2}$$

in which N_{cl}^{j} is the total number of atoms of species j found in clusters and $\sum N_{\text{cl}}$ is the total number of atoms found in clusters. To initiate the calculation, values from the as-received condition are used. However, since HCM12A does not contain pre-existing nanoclusters in the as-received specimens, the values for r, n, and p are initially 0, and values for C are estimated as the sum of the bulk concentration for each clustering solute.

The most difficult parameter to estimate for the model is the disordering parameter ($\psi = l \cdot f$), which comprises the effective cascade diameter (l) and the disordering efficiency (f). Although we have previously attempted a simplified method to approximate values of l for Fe^{2+} (6.6 nm), proton (2.3 nm), and neutron irradiation (9.3 nm) conditions[19] to isolate f, we will use the whole disordering parameter (Ψ) as a fitted variable.

Finally, the RED rate (D_j^{irr}) for the solutes species (j) in question may be estimated through comparison of the equilibrium and irradiation-induced vacancy concentrations as:

$$D_j^{\text{irr}} = \frac{C_v^{\text{irr}}}{C_v^{\text{eq}}} D_j^{th} \tag{3}$$

which is the same approach to that taken in Ref. 28–30 In Eq. 3, C_v^{irr} is the non-equilibrium concentration of vacancies due to irradiation ($C_v^{\text{irr}} = K\tau$),[29] in which K is the dose rate of irradiation (dpa/s), and τ is the characteristic time for vacancy defects to migrate to a sink in the microstructure:[29]

$$\tau = \frac{1}{k_{\text{total}}^2 D_v} \tag{4}$$

Here, τ is dependent on the microstructure sink strength for the target alloy (k^2) and the vacancy diffusion coefficient (D_v). Refer to online supplementary material for the approach for determining sink strength (ESM Sec. A). Meanwhile, C_v^{eq} is the thermal vacancy concentration at equilibrium when irradiation is absent. Finally, thermal diffusion (D_j^{th}) for solutes is:

$$D_j^{\text{th}} = D_j^0 \exp\left(-\frac{E_j^m}{k_b T}\right) \tag{5}$$

where D_j^0 is the pre-exponential, E_j^m is the migration energy, k_b is Boltzmann's constant, and T is irradiation temperature. Using substitutions, Eq. 3 is rewritten as:

$$D_j^{\text{irr}} = \frac{K}{k_{\text{total}}^2 D_v} \frac{D_j^{\text{th}}}{C_v^{\text{eq}}} \tag{6}$$

Values for the solute-specific variables are retrieved for each respective solute from the literature as initial estimates (Table III).[5,23,31–33] For the ODS alloy, diffusion parameters for interstitial O are not considered since previous studies show

Table III. Initial thermal diffusion parameters applied for this study

Solute(s)	Pre-exponential, D_0 (cm^2/s)	Migration energy, E_j^m (eV)	Calculated D_j^{th} (cm^2/s) at 500°C	Source
Fe-9%Cr ODS				
Y	0.1	3.25	6.24×10^{-22}	5
Ti	2100	3.04	3.29×10^{-17}	5,31,32
Y + Ti	Fitted	3.10	Fitted	This study
HCM12A				
Si	0.78	2.40	1.85×10^{-16}	23
Mn	1.49	2.43	2.16×10^{-16}	23
Ni	1.4	2.55	3.35×10^{-17}	23
Si + Mn + Ni	Fitted	2.48	Fitted	This study
Cu	6.1	2.78	4.63×10^{-18}	33

that O is not a limiting reagent for the formation of Y-Ti-O-rich nanoclusters in ODS alloys.[19,34] Since the migration energies for each solute in the ODS and HCM12A are similar in magnitude, a weighted average for the migration energy is estimated based on the non-carbide solute concentrations (C_j), respectively for each solute (Table II). This weighted-average approach was less effective for the pre-exponential parameters, and so the combined pre-exponential terms for thermal diffusion were fitted along with the disordering parameter (Ψ).

Initially, Eq. 1 is applied to the as-received nanocluster morphology and the respective parameters of each irradiation (Fe^{2+}, proton, or neutron) separately. Values for dr/dt are calculated for each irradiation and applied over a finite amount of time, Δt, after which a new nanocluster radius is determined. Using this revised nanocluster radius, a new microstructure sink strength is estimated following Eqs. S-8 and S-12. Subsequently, the characteristic time (τ), the radiation-induced concentration of vacancies (C_v^{irr}), and the RED (D_j^{irr}) are updated accordingly. This stepwise calculation is repeated over the same finite time intervals, incrementally accumulating more "dose" with increasing time. Details about each subroutine and a flow chart of the model logic are outlined in ESM Sec. B.

Application and Sensitivity

The first system modeled is the Fe-9%Cr ODS alloy, which contains a high density of oxide nanoclusters before irradiation. The initial model parameters for each irradiation are provided in Table IV. Initially, values for Ψ_p and D^0_{Y-Ti} are co-fitted using the experimental nanocluster size data following proton irradiation to 1 dpa, 3 dpa, and 7 dpa at 500°C (Table II). Next, using the same D^0_{Y-Ti} fitted parameter, values for Ψ_{Fe} and Ψ_n are fitted using empirical data following each irradiation, respectively (Table II).

A complete sensitivity analysis is conducted to identify the relative influence of each input parameter (P) on the output, which is taken as the steady-state cluster size (d_{ss}). Sensitivity analysis highlights parameters to which d_{ss} is most sensitive and is the derivative of the output as a function of the input parameter ($\delta d_{ss}/d_P$). The approach taken is to vary the input parameter about its reference value and solve for sensitivity using:

$$\frac{\delta d}{\delta P} = \frac{d'_{ss} - d^{ref}_{ss}}{P' - P^{ref}} \tag{7}$$

where d^{ref}_{ss} is the calculated steady-state cluster diameter using the reference input parameter (P^{ref}). With P' as the varied parameter, d'_{ss} is the new steady-state cluster diameter. Sensitivity is expressed as a significance, S^d_P, giving a more straightforward comparison of the relative influence of each variable:

$$S^d_P = \frac{d'_{ss} - d^{ref}_{ss}}{P' - P^{ref}} \cdot \frac{P^{ref}}{d^{ref}_{ss}} \tag{8}$$

Variables exhibiting the highest significance are those to which the model is most sensitive.

The significance is determined for each variable via simulation of proton-irradiation on the Fe-9%Cr ODS alloy at 500°C. The predicted steady-state cluster diameter for this set of conditions is $d^{ref}_{ss} = 5.32$ nm. Each variable is altered with values slightly higher than the reference value for the parameter, and the significance is calculated and illustrated in Fig. 1. Variables with a negative significance indicate that an increase in the parameter value will result in a decrease in the predicted steady-state cluster size.

Interestingly, the initial cluster size (r) does not influence the predicted irradiation-induced stable cluster size. The model instead predicts a stable size based on the balance of the other parameters and will predict evolution toward this

Table IV. Initial parameters in the NHM model for Fe-9%Cr ODS and HCM12A simulations

		Fe-9%Cr ODS			HCM12A			
Parameter	**Units**	**Fe^{2+} irradiation**	**Proton irradiation**	**Neutron irradiation**	**Fe^{2+} irradiation**	**Proton irradiation**	**Neutron irradiation**	**Source**
K	dpa/s	2.23×10^{-4}	1.2×10^{-5}	1×10^{-7}	2.23×10^{-4}	1.2×10^{-5}	1×10^{-7}	19
$\phi = K(10^{14})$	atoms/cm^2-s	2.23×10^{10}	1.20×10^{9}	1.00×10^{7}	2.23×10^{10}	1.20×10^{9}	1.00×10^{7}	19
N	atoms/nm^3	85.2	85.2	85.2	85.2	85.2	85.2	–
Ψ	nm	0.26	0.34	0.43	0.58	0.74	1.21	Fitted
k^2	cm^{-2}	2.70×10^{12}	2.70×10^{12}	2.70×10^{12}	2.90×10^{11}	2.90×10^{11}	2.90×10^{11}	Eq. SI-8
T	K	773	773	773	773	773	773	19
$E^m_{Y,Ti}$	eV	3.10	3.10	3.10	–	–	–	Table III
$E^m_{Si,Mn,Ni}$	eV	–	–	–	2.48	2.48	2.48	Table III
E^m_{Cu}	eV	–	–	–	2.78	2.78	2.78	Table III
$D^0_{Y,Ti}$	cm^2/s	0.613	0.613	0.613	–	–	–	Fitted
$D^0_{Si,Mn,Ni}$	cm^2/s	–	–	–	1.4×10^{-4}	1.4×10^{-4}	1.4×10^{-4}	Fitted
D^0_{Cu}	cm^2/s	–	–	–	3.0×10^{-2}	3.0×10^{-2}	3.0×10^{-2}	Fitted
E^f_v	eV	2.2	2.2	2.2	1.65	1.65	1.65	23,29,36
E^m_v	eV	0.68	0.68	0.68	0.68	0.68	0.68	35
r	nm	2.855	2.855	2.855	0.0	0.0	0.0	Table II
n	m^{-3}	4.43×10^{23}	4.43×10^{23}	4.43×10^{23}	0.0	0.0	0.0	Table II
$p_{Y\text{-}Ti}$	–	0.0873	0.0873	0.0873	–	–	–	19
$p_{Si,Mn,Ni}$	–	–	–	–	0.001	0.001	0.001	–
p_{Cu}	–	–	–	–	0.001	0.001	0.001	–
$C_{Y\text{-}Ti}$	–	0.0062	0.0062	0.0062	–	–	–	19
$C_{Si,Mn,Ni}$	–	–	–	–	0.0212	0.0212	0.0212	19
C_{Cu}	–	–	–	–	0.0132	0.0132	0.0132	19
Δt	s	1200	14,400	1,440,000	1200	14,400	1,440,000	This study

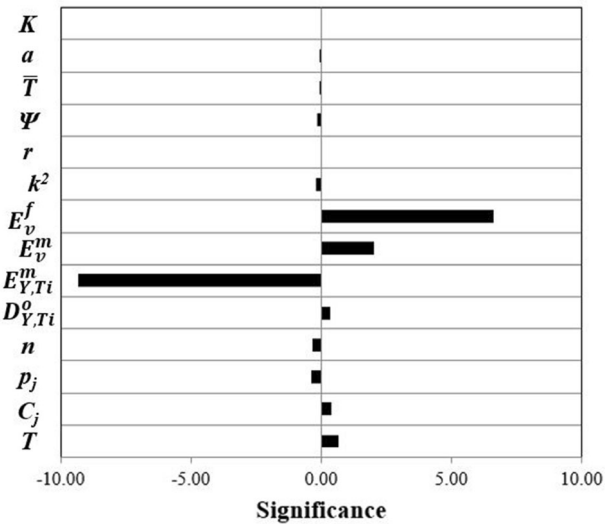

Fig. 1. Significance of each parameter on the predicted stable nanocluster size using the NHM model for simulating proton-irradiated Fe-9%Cr ODS.

stable size, regardless of the starting point. Similarly, steady-state particle size is independent of irradiation dose rate, which may seem counterintuitive. However, dose rate (K) is embedded in the numerator of each term on the right-hand side of Eq. 1, offsetting their effects on the outcome. Therefore, differences in steady-state cluster size due to differing irradiation particles is determined only by the cascade morphology and efficiency (dissolution parameter) in the model (ψ in Eq. 1), and the irradiation temperature (T).

From Fig. 1, the solute migration energy (E^m_j) is the most significant parameter influencing the model, and is far more significant than the fitted parameters (Ψ and D^0_j). Figure 1 also shows that the vacancy formation (E^f_v) and vacancy migration (E^m_v) energies are also influential. One key difference is the respective directions of the sensitivity for these three parameters. The root of this relationship is in Eq. 6, which can be rewritten as:

$$D^{\text{irr}}_j = D^0_{\text{comb}} \exp\left(\frac{-E^m_j + E^f_v + E^m_v}{k_b T}\right) \quad (9)$$

where D^0_{comb} is the combined pre-exponential, while each activation energy appears in the numerator of the exponential. The sign of this numerator indicates the direction of temperature sensitivity. Specifically, if the sum $(-E^m_j + E^f_v + E^m_v)$ is negative,

as is the case for Fe-9%Cr ODS ($-3.1 + 2.2 + 0.68 = -0.22$ eV)[29,35] and HCM12A ($-2.48 + 1.65 + 0.68 = -0.15$ eV),[23,35,36] higher irradiation temperature will result in larger nanoclusters. However, if this numerator is positive, nanocluster size as a function of temperature will exhibit the opposite trend. As will be discussed further in "Results and Discussion" section, the sign of this numerator has profound implications on the "temperature shift," used to account for differences in point defect diffusivity under variable irradiation dose rates and/or particle types.[37,38] This realization further emphasizes the importance of having high confidence in the estimates for these activation energies to ensure usefulness of the model.

The next system modeled is the HCM12A alloy. A summary of initial parameters for each irradiation is provided in Table IV. Two separate calculations are conducted to simulate nanocluster evolution for the Si-Mn-Ni-rich clusters and Cu-rich clusters, respectively. Because the alloy does not contain any pre-existing nanoclusters, values for r, n, and p are set to 0. But the NHM model requires some inherent nanoclusters to be present, so the initial value of p is set to 0.001 and an artificial "nucleation" event is introduced by manually setting the value of r to ~ 1.0 nm (roughly equivalent to the smallest nanoclusters identified via APT). The timing for introducing nucleation depends on the empirical information available, providing information about the approximate dose at which cluster nucleation likely occurs. In HCM12A, after proton irradiation to 1 dpa, only Cu-rich clusters are present, suggesting that Cu-rich clusters nucleate prior to 1 dpa. However, after proton irradiation to 2.4 dpa, both Cu-rich clustering and Si-Mn-Ni-rich clusters are present, suggesting that Si-Mn-Ni-rich clusters nucleate between 1 dpa and 2.4 dpa. As a result, Cu cluster nucleation is introduced in the model at ~ 0.5 dpa, while Si-Mn-Ni cluster nucleation is introduced at ~ 1.5 dpa.

RESULTS AND DISCUSSION

For the ODS alloy, NHM model predictions (using fitted parameters) are plotted as lines for comparison with measured cluster sizes following each irradiation experiment in Fig. 2a. For all three irradiations, predicted average cluster size approaches a steady state (i.e., < 0.001 nm change in r per Δt) within the first few 3–7 dpa. Each calculation is fitted to the experimental data as closely as possible using disordering efficiencies of $\Psi^{Fe}_{Y,Ti} = 0.26$ nm, $\Psi^{p}_{Y,Ti} = 0.34$ nm, and $\Psi^{n}_{Y,Ti} = 0.43$ nm, respectively, and a common value of $D^{0}_{Y,Ti} = 0.613\,cm^2/s$.

NHM model predictions for HCM12A are plotted as lines for comparison with measured cluster sizes following each irradiation experiment in Fig. 2b and c. For all three irradiations, the average size of Si-

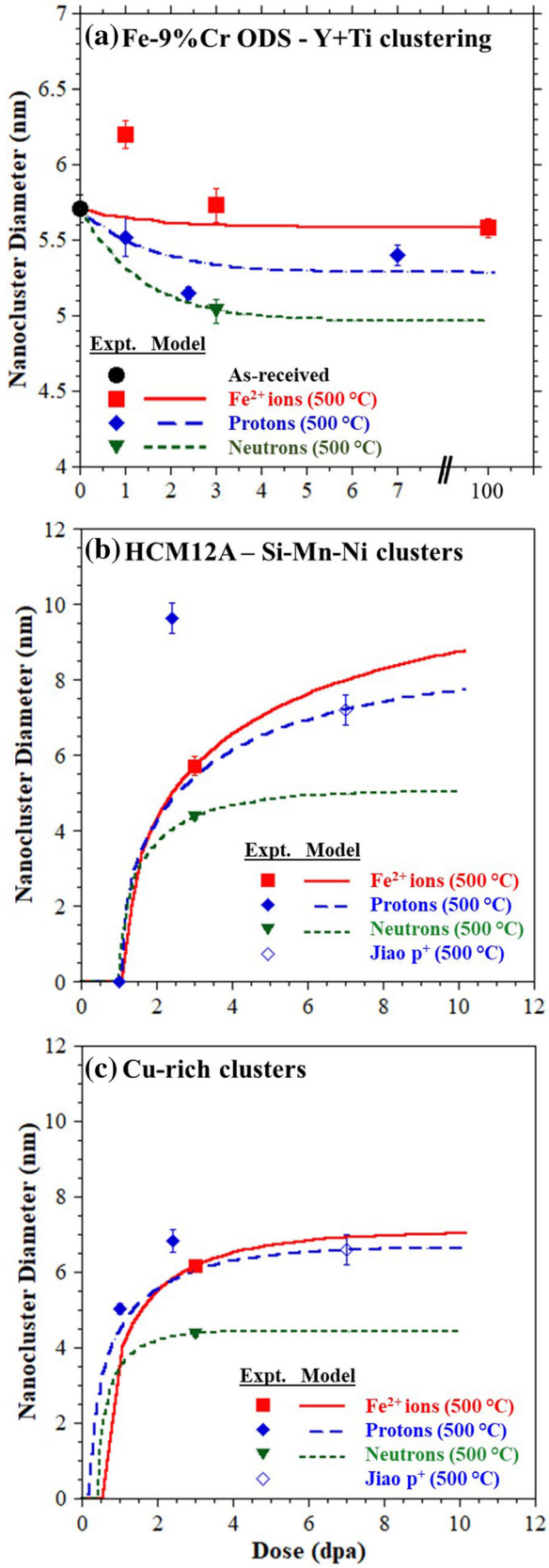

Fig. 2. NHM simulations of solute clustering in (a) Y + Ti solutes in Fe-9%Cr ODS, (b) Si-Mn-Ni solutes in HCM12A, and (c) Cu solutes in HCM12A.

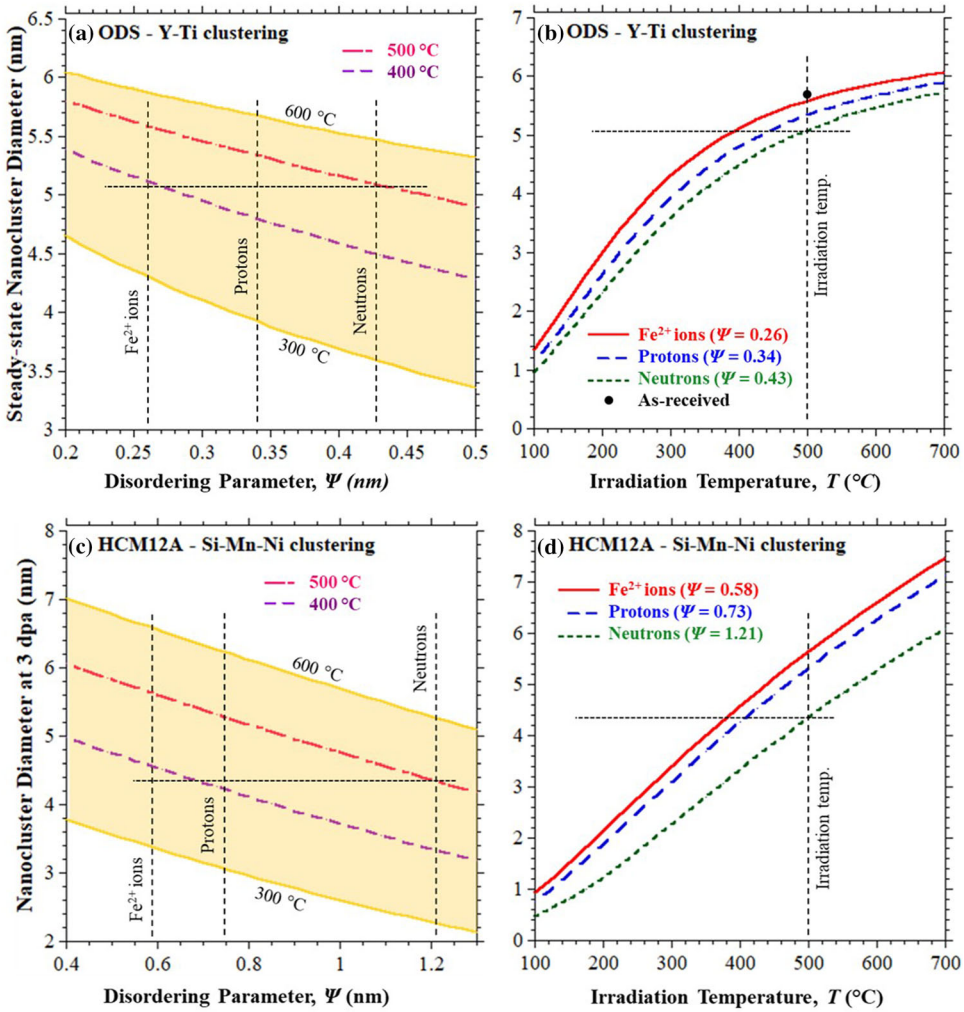

Fig. 3. Solution space for the NHM equation (Eq. 1) for a range of irradiation temperatures and disordering parameters (Ψ) in (a, b) Fe-9%Cr ODS with Y-Ti clustering, and (c, d) HCM12A with Si-Mn-Ni clustering. Horizontal dashed lines enable identification of parameters needed to emulate neutron irradiation results.

Mn-Ni-rich and Cu-rich clusters grows quickly after nucleation and evolves toward a steady state (i.e., ≤ 0.001 nm change in r per Δt) within the first ~ 40 dpa. Each calculation is fitted to the experimental cluster size measurement at the highest dose. For the Si-Mn-Ni clusters, the fitted disordering efficiencies are $\Psi^{Fe}_{Si,Mn,Ni} = 0.58$ nm, $\Psi^{p}_{Si,Mn,Ni} = 0.74$ nm, and $\Psi^{n}_{Si,Mn,Ni} = 1.21$ nm, respectively, with $D^{0}_{Si,Mn,Ni} = 1.4 \times 10^{-4}\,cm^2/s$. For the Cu-rich clusters, the disordering efficiencies are $\Psi^{Fe}_{Cu} = 1.21$ nm, $\Psi^{p}_{Cu} = 1.37$ nm, and $\Psi^{n}_{Cu} = 2.06$ nm, respectively, with $D^{0}_{Cu} = 4 \times 10^{-2}\,cm^2/s$. Experimentally, both Fe^{2+} irradiation in ODS and proton irradiation in HCM12A exhibit temporary increases in nanocluster diameter at low dose, suggesting that these are not steady-state phenomena. The NHM model is not able to simulate this effect, as it only seeks the steady-state balance between the irradiation-induced dissolution and growth effects.

The fitted values for the pre-exponential (D^0_j) of the thermal diffusion of each respective solute group (Table IV) are generally lower than accepted values (except for Y) in the literature (Table III). It is unclear why this is, but it may reflect the relative affinity of the solutes to the clusters in question. Previous studies of ODS alloys have shown oxide precipitation is driven by strong thermodynamic forces including a large enthalpy of formation and low solubility of Y.[31] Meanwhile, the clustering of Si, Mn, and Ni elements are likely a result of radiation-induced segregation,[18] which is likely a weaker driving force for solute clustering.

The fitted values for Ψ are consistently highest with neutron irradiation for all three solute cluster types. This may result from the neutron irradiation damage cascade morphology, but is also likely due to the lower dose rate of neutron irradiation, which enables any disordering diffusion to fully occur following a cascade before the next cascade is created. Meanwhile, the lowest fitted values for Ψ

are consistently for Fe^{2+} irradiation, which may be due to the higher dose rate which limits disordering diffusion. Finally, proton irradiation values for Ψ are consistently in the middle. While proton irradiation cascades are typically much smaller in size, they are also estimated to be more efficient at creating defects[39] and the dose rate is typically lower than with heavy ions.

Plots of the NHM model solution space for both the ODS and HCM12A alloys are provided in Fig. 3 across a range of disordering parameters (Ψ) and irradiation temperatures. These plots are created by conducting over 775 iterative simulations for each alloy, with each iteration taking ~ 10 s to run and record the result. Dashed lines are provided at the disordering parameters for each respective irradiation and for comparison of parameter combinations enabling emulation of neutron size evolution. Smaller values for Ψ will reduce the dissolution effects of irradiation. Therefore, a lower temperature is needed to simultaneously reduce corresponding irradiation-induced growth and still achieve comparable cluster sizes. While the direction of this shift is contradictory to Mansur's invariance theory, it is consistent with a theory by Martin[30] to describe nanocluster evolution upon irradiation with different dose rates. Martin proposes that increased irradiation dose rate causes an increase in the configurational entropy of the system, analogous to a rise in temperature. With this temperature dilation, higher rates of RED are expected, favoring nanocluster growth. As a result, the Martin theory suggests higher dose rate irradiations may need to be conducted at lower temperatures to limit solute mobility and attain more consistent nanocluster morphologies.

Nanocluster evolution predictions trend toward a steady-state average size. This steady-state is achieved when the competing effects of ballistic dissolution and diffusion-driven growth are in balance. By rearranging Eq. 1 with $dr/dt = 0$, the predicted steady-state average nanocluster size, r, may be expressed as a function of the irradiation temperature. These functions are plotted in Fig. 4 for the ODS alloy and each irradiating particle (Fe^{2+} ions, protons, and neutrons). A vertical dashed line is provided at 500°C to highlight the results measured and modeled in this study. A horizontal dashed line is provided at $r = 2.855$ nm, the initial average size of ODS nanoclusters before irradiation. The points where this horizontal line crosses each curve represent the predicted irradiation temperature which would enable cluster size stability. Unfortunately, a plot of this nature is less meaningful for HCM12A since there are no clusters present in the as-received condition.

Both views of the solution space for the NHM model in Fe-9%Cr ODS and HCM12A predict a negative temperature shift for charged particles (with smaller Ψ values) to emulate solute cluster evolution from neutron irradiation. Therefore, the Ψ parameter, which quantifies the disordering

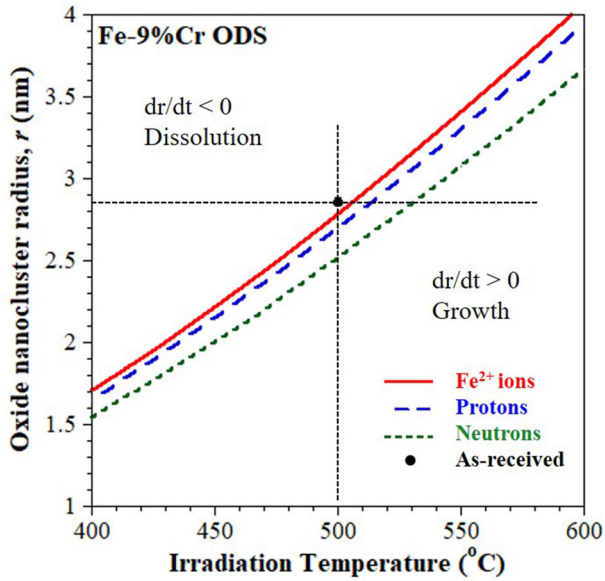

Fig. 4. Comparison of steady-state oxide nanocluster size (r) versus irradiation temperature for each irradiating particle in Fe-9%Cr ODS.

efficiency of irradiation, reflects the influence of both the irradiating particle and the respective dose rate of irradiation. It is important to recognize that Martin's temperature dilation theory was developed to describe solute phase evolution upon irradiation, while the Mansur invariance theory was developed in the context of defect clusters (i.e., voids). The basis of the invariance theory is to equate the concentration of vacancies within the microstructure. With higher dose rates producing a higher density of defects (in less time), this effect must be offset by increasing the irradiation temperature. The higher temperature increases defect mobility, causing more trapping and annihilation at sinks and balancing the increase in defect production rate. As a result, the invariance theory (which predicts a positive temperature shift of + 50°C to 60°C) likely still applies for defect clusters such as dislocation loops and voids. In fact, Taller et al.[40] conducted a systematic study on F/M alloy T91 (which is very similar to HCM12A) using a range of positive temperature shifts and found good agreement in dislocation loop morphologies and cavity size distribution using a temperature shift of + 60°C to 70°C. Unfortunately, they did not find the same match in nanocluster morphology, suggesting a need for feature-specific temperature shifts, which has also been hypothesized in Ref. 41.

To check the negative shift prediction, we can use the data from Jiao et al.[13] for proton irradiation of HCM12A at 400°C (Table II). This data is plotted in Fig. 5 along with the model prediction for proton irradiation at 400°C. Empirical and simulation results for Si-Mn-Ni clusters correlate well with neutron irradiation results at 500°C, while the Cu-rich simulation does not match up with the data

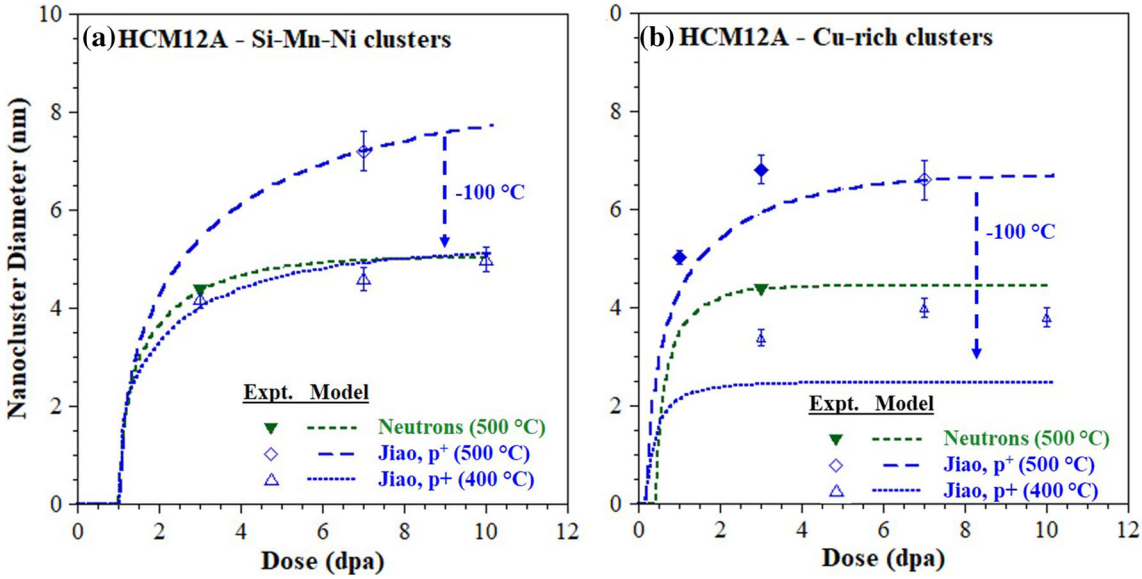

Fig. 5. NHM simulations of clustering in HCM12A clustering for (a) Si-Mn-Ni clusters, and (b) Cu-rich clusters, evaluating proton irradiation at 400°C as an emulation for neutron irradiation at 500°C.

nearly as well. The reason for this slight mismatch is unclear but may be related to the formation mechanism of the clusters. Cu is known to have low solubility in b.c.c. Fe, resulting in Cu precipitation even in the absence of irradiation.[42,43] Recently, a similar study using cluster dynamics to simulate Si-Mn-Ni clusters in F/M alloy T91[44] also predicted a comparable negative temperature shift of ~ -120°C for Fe^{2+} irradiation to emulate neutron irradiation at 500°C.

In our experience, each iteration with cluster dynamics takes $\sim$ 7 days to 10 days to simulate a dosage up to 3 dpa, while the NHM calculation is instantaneous, allowing quick sensitivity and optimization feedback. In application, one might consider using both models for simulation purposes: (1) using the NHM model to quickly optimize a given parameter, followed by (2) using cluster dynamics to validate the prediction using a correlative input.

Finally, to enable broader utilization of the NHM model, we have created a simple user interface for parameter entry and plotting of prediction results.[45] More details about the user-friendly version of the NHM model may be found in EMS Sec. C.

CONCLUSION

We advance a rate theory model to simulate irradiation-induced nanocluster evolution for different irradiating particles. While this model is not as computationally rigorous as other established models, the advantage of this simple model is primarily in its agility. Iterative calculations may be done instantaneously, enabling swift evaluation of parameter sensitivity, optimization, and alloy screening.

Using the NHM model, nanocluster evolution is found to depend upon the disordering parameter (i.e., cluster morphology) and irradiation temperature and is most sensitive to the solute migration, vacancy formation, and vacancy migration energies. Investigation of the solution space for solute cluster evolution suggests a negative temperature shift is required for higher dose rate irradiating particles to emulate low dose rate neutron irradiation for Y-Ti-O-rich, Si-Mn-Ni-rich, and Cu-rich clusters in the b.c.c. Fe matrix.

ACKNOWLEDGEMENTS

This manuscript is partly based on work done while the primary author was a graduate student at Boise State University. The authors acknowledge Didier Ishimwe for creating the user-friendly version of the NHM model available on NanoHub. This research was sponsored in part by the US Nuclear Regulatory Commission Grants NRC-HQ-84-14-G-0056 and NRC-HQ-84-15-G-0025, the Micron Foundation, and by the US DOE, Office of Nuclear Energy under DOE Idaho Operations Office Contract DE-AC07-05ID14517, as part of the Nuclear Science User Facilities experiments 13-419, 14-486, 15-540, 15-569, 16-625, 16-710, 18-1210, and 19-1765.

ELECTRONIC SUPPLEMENTARY MATERIAL

The online version of this article (https://doi.org/10.1007/s11837-020-04365-4) contains supplemen-

tary material, which is available to authorized users.

REFERENCES

1. A. Certain, S. Kuchibhatla, V. Shutthanandan, D.T. Hoelzer, and T.R. Allen, *J. Nucl. Mater.* 434, 311 (2013).
2. A.G. Certain, K.G. Field, T.R. Allen, M.K. Miller, J. Bentley, and J.T. Busby, *J. Nucl. Mater.* 407, 2 (2010).
3. J. He, F. Wan, K. Sridharan, T.R. Allen, A. Certain, V. Shutthanandan, and Y.Q. Wu, *J. Nucl. Mater.* 455, 41 (2014).
4. J. He, F. Wan, K. Sridharan, T.R. Allen, A. Certain, and Y.Q. Wu, *J. Nucl. Mater.* 452, 87 (2014).
5. C. Hin and B.D. Wirth, *J. Nucl. Mater.* 402, 30 (2010).
6. C. Liu, C. Yu, N. Hashimoto, S. Ohnuki, M. Ando, K. Shiba, and S. Jitsukawa, *J. Nucl. Mater.* 417, 270 (2011).
7. T. Chen, E. Aydogan, J.G. Gigax, D. Chen, J. Wang, X. Wang, S. Ukai, F.A. Garner, and L. Shao, *J. Nucl. Mater.* 467, 42 (2015).
8. M.B. Toloczko, F.A. Garner, V.N. Voyevodin, V.V. Bryk, O.V. Borodin, V.V. Mel'Nychenko, and A.S. Kalchenko, *J. Nucl. Mater.* 453, 323 (2014).
9. J.P. Wharry, M.J. Swenson, and K.H. Yano, *J. Nucl. Mater.* 486, 11 (2017).
10. P.D. Edmondson, C.M. Parish, and R.K. Nanstad, *Acta Mater.* 134, 31 (2017).
11. O. Anderoglu, J. Van Den Bosch, P. Hosemann, E. Stergar, B.H. Sencer, and D. Bhattacharyya, *J. Nucl. Mater.* 430, 194 (2012).
12. E. Getto, K. Sun, A.M. Monterrosa, Z. Jiao, M.J. Hackett, and G.S. Was, *J. Nucl. Mater.* 480, 159 (2016).
13. Z. Jiao and G.S. Was, *J. Nucl. Mater.* 425, 105 (2012).
14. Z. Jiao, V. Shankar, and G.S. Was, *J. Nucl. Mater.* 419, 52 (2011).
15. A.V. Barashev, S.I. Golubov, D.J. Bacon, P.E.J. Flewitt, and T.A. Lewis, *Acta Mater.* 52, 877 (2008).
16. T.R. Allen, J.P. Wharry, K.G. Field, D.L. Morgan, A.T. Motta, B.D. Wirth, and Y. Yang, *J. Mater. Res.* 30, 1246 (2015).
17. T.R. Allen, L. Tan, J. Gan, G. Gupta, G.S. Was, E.A. Kenik, S. Shutthanandan, and S. Thevuthasan, *J. Nucl. Mater.* 351, 174 (2006).
18. J.P. Wharry, Z. Jiao, V. Shankar, J.T. Busby, and G.S. Was, *J. Nucl. Mater.* 417, 140 (2011).
19. M.J. Swenson and J.P. Wharry, *J. Nucl. Mater.* 496, 24 (2017).
20. J. Ribis, E. Bordas, P. Trocellier, Y. Serruys, Y. de Carlan, and A. Legris, *J. Mater. Res.* 30, 2210 (2015).
21. D. Xu, A. Certain, H.L. Voigt, T. Allen, B.D. Wirth, D. Xu, A. Certain, H.L. Voigt, T. Allen, and B.D. Wirth, *J. Chem. Phys.* 145, 104704 (2016).
22. T. Schuler, M. Nastar, and F. Soisson, *Phys. Rev. B.* 14113, 1 (2017).
23. H. Ke, P. Wells, P.D. Edmondson, N. Almirall, L. Barnard, G.R. Odette, and D. Morgan, *Acta Mater.* 138, 10 (2017).
24. T.R. Allen and G.S. Was, *Acta Mater.* 46, 3679 (1998).
25. J.P. Wharry, Z. Jiao, and G.S. Was, *J. Nucl. Mater.* 425, 117 (2012).
26. J.P. Wharry and G.S. Was, *Acta Mater.* 65, 42 (2014).
27. R.S. Nelson, J.A. Hudson, and D.J. Mazey, *J. Nucl. Mater.* 44, 318 (1972).
28. C. Flament, J. Ribis, J. Garnier, Y. Serruys, F. Leprêtre, A. Gentils, C. Baumier, M. Descoins, D. Mangelinck, A. Lopez, K. Colas, K. Buchanan, P. Donnadieu, and A. Deschamps, *Acta Mater.* 128, 64 (2017).
29. M.-L. Lescoat, J. Ribis, Y. Chen, E.A. Marquis, E. Bordas, P. Trocellier, Y. Serruys, A. Gentils, O. Kaïtasov, Y. de Carlan, and A. Legris, *Acta Mater.* 78, 328 (2014).
30. G. Martin, *Phys. Rev. B.* 30, 1424 (1984).
31. L. Barnard, N. Cunningham, G.R. Odette, I. Szlufarska, and D. Morgan, *Acta Mater.* 91, 340 (2015).
32. X. Boulnat, M. Perez, D. Fabregue, S. Cazottes, and Y. De Carlan, *Acta Mater.* 107, 390 (2016).
33. W. Gale and T. Totemeier, *Smithells Metals Reference Book*, 8th ed. (Amsterdam: Elsevier, 2004).
34. M.J. Swenson and J.P. Wharry, *J. Nucl. Mater.* 467, 97 (2015).
35. C. Hofer, E. Stergar, S.A. Maloy, Y.Q. Wang, and P. Hosemann, *J. Nucl. Mater.* 458, 361 (2015).
36. J. Ke, H. Ke, G.R. Odette, and D. Morgan, *J. Nucl. Mater.* 498, 83 (2018).
37. L.K. Mansur, *J. Nucl. Mater.* 206, 306 (1993).
38. L.K. Mansur, *J. Nucl. Mater.* 78, 156 (1978).
39. G.S. Was, *Fundamentals of Radiation Materials Science: Metals and Alloys*, 2nd ed. (Berlin: Springer, 2017).
40. S. Taller, Z. Jiao, K. Field, and G.S. Was, *J. Nucl. Mater.* 527, 151831 (2019).
41. S.J. Zinkle and L.L. Snead, *Scr. Mater.* 143, 154 (2018).
42. S. Cui, M. Mamivand, and D. Morgan, *Mater. Des.* 191, 108574 (2020).
43. F. Soisson and C.C. Fu, *Phys. Rev. B - Condens. Matter Mater. Phys.* 76, 1 (2007).
44. S.B. Adisa, R. Blair, and M.J. Swenson, *Materialia* 12, 100700 (2020).
45. D. Ishimwe, M.J. Swenson, and J.P. Wharry, https://nanohub.org/tools/ncevol. Accessed Aug 2020.